

# Self-Assembled Monolayers of Hexapeptides on Gold: Surface Characterization and Orientation Distribution Analysis<sup>†</sup>

Xingu Wen, Richard W. Linton, Fernando Formaggio,<sup>‡</sup> Claudio Toniolo,<sup>‡</sup> and Edward T. Samulski\*

Department of Chemistry, CB# 3290, University of North Carolina at Chapel Hill, Chapel Hill, North Carolina 27599-3290

Received: May 14, 2004; In Final Form: July 28, 2004

Monodisperse hexapeptides that have lipoic acid coupled to the N-terminus were self-assembled on gold substrates. The self-assembled monolayer (SAM) film compositions were investigated by X-ray photoelectron spectroscopy (XPS), angle dependent XPS, and grazing angle Fourier transform infrared reflection–absorption spectroscopy (FTIR–RAS). The surface coverage of the self-assembled films was significantly larger than that of control physisorbed films, and the chemisorption between the hexapeptides and gold surface was stable in solvent. The structural results indicated that the hexapeptides helix orientation distribution relative to the surface normal is ambiguous—the data can be explained by either a broad distribution of an on-average perpendicular arrangement or a tight distribution about a single tilt angle. Hexapeptides in which a spin label, 2,2,6,6-tetramethylpiperidine-1-oxyl-4-amino-4-carboxylic acid (TOAC), was incorporated as an amino acid residue exhibit electron spin resonance (ESR) spectra dominated by spin-exchange broadening. This broadening precluded the possibility of using ESR evidence to get insights into hexapeptide orientational order from simulated spectra. ESR suggests that when the spin-label-containing hexapeptide is diluted in the SAM, orientational order is not apparent; the labeled hexapeptide SAM is disordered either structurally or conformationally or both.

## Introduction

Self-assembled monolayers (SAMs) of organosulfur compounds on gold continue to be extensively used as a platform for surface modification.<sup>1</sup> More than two decades after Nuzzo and Allara first reported the formation of SAMs by the spontaneous adsorption of dialkyl disulfides on gold,<sup>2</sup> many reports have appeared about SAMs having different thicknesses (chain lengths) and exterior surface functionalities.<sup>3–12</sup> A decade ago, Enriquez et al. showed that  $\alpha$ -helical oligopeptides containing a disulfide moiety can also be self-assembled on gold.<sup>13,14</sup> As stated by the authors, their motivation for fabricating polypeptide SAMs was to exploit unique features of polypeptide primary and secondary structures: They observed that via either the Merrifield protocol<sup>15</sup> or genetic expression,<sup>16</sup> it would be possible to create a designed peptide sequence—a sequence of side chains with specified functionality—that in turn would be manifested in the SAM as spatially resolved, chemically distinct functionalities localized in a series of strata coplanar with the substrate (Figure 1). And moreover, the macrodipole moment associated with the vector sum of individual peptide dipoles in the  $\alpha$ -helical secondary structure was anticipated to give rise to an intrinsically polar SAM. Enriquez et al. speculated that such polar films might, for example, facilitate light-induced electron–hole separation for appropriately placed chromophores.<sup>13,14</sup> Those speculations appear to have been confirmed by the subsequent findings of Miura et al.<sup>17</sup> who reported significant surface potentials for oriented polypeptide SAMs,

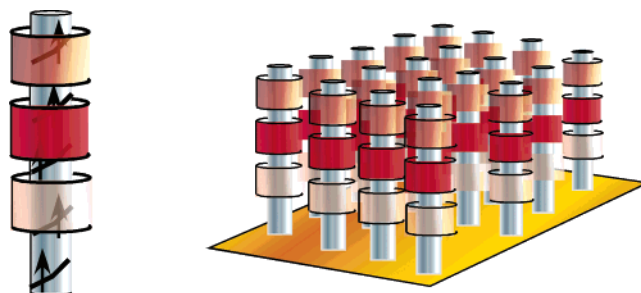


**Figure 1.** Schematic illustration of an ideal oligopeptide helix with variable side chains (left) and a self-assembled monolayer of oligopeptides on gold (right). Peptide dipoles point in the same sense along the helix axis.

and by the reports of photocurrent generation from carbazole side chains in polypeptide SAMs.<sup>18,19</sup> Several routes to polypeptide SAMs have been reported: surface grafting schemes on gold and other substrates,<sup>20–22</sup> chemisorption of disulfide-labeled oligopeptides on gold,<sup>13,14,23–25</sup> and complex ion-pair formation between peptides and end-functionalized, preformed SAMs.<sup>26,27</sup>

The polypeptide SAMs fabricated by Enriquez et al.<sup>13,14</sup> employed polydisperse samples, i.e., commercial, base-initiated polypeptides with a wide distribution of molecular weights (helix lengths). In turn, the length polydispersity was believed to be the origin of the rather low degrees of helix axis orientational order inferred from Fourier transform IR reflection–absorption spectroscopy (FTIR–RAS) studies of those polypeptide SAMs. The observed ratios,  $D$ , of the amide I to the amide II band intensity were fit with broad, Gaussian-distributed helix axis orientations.<sup>14</sup> Herein we examine the nature of polypeptide order in SAMs composed of monodisperse hexapeptides (Figure 2). All are hexapeptides that contain  $\alpha$ -aminoisobutyric acid

<sup>†</sup> Part of the special issue “Tomas Baer Festschrift”.

\* Corresponding author. E-mail: et@unc.edu.

<sup>‡</sup> Department of Organic Chemistry, University of Padova, Via Marzolo, 1, 35131 Padova, Italy.



**TABLE 1: XPS Atomic Concentrations (%) Acquired at a Take-Off Angle of 75° for Self-assembled Hexapeptide B and Hexapeptide C Films and Physisorbed Hexapeptide A Film**

film	C	O	N	S
peptide B	70.4 ± 1.6	14.3 ± 0.8	11.3 ± 0.7	4.0 ± 0.2
theory	69.2	15.4	11.5	3.9
peptide C	69.7 ± 1.0	14.9 ± 0.5	11.9 ± 0.6	3.5 ± 0.2
theory	69.0	15.5	12.1	3.4
peptide A	72.5 ± 1.3	16.1 ± 0.6	11.4 ± 0.4	
theory	70.6	17.6	11.8	

The hexapeptide film was placed in the ESR cavity with the film surface parallel or perpendicular to the magnetic field. The center field was 3315 G and the microwave frequency was 9.365 GHz.

## Results and Discussion

**Film Composition.** The elements characteristic of the three hexapeptides (C, O, and N) were detected in XPS for both SAMs of hexapeptide B and hexapeptide C and physisorbed hexapeptide A films. As expected, S was only detected in the hexapeptide B and hexapeptide C SAMs. Table 1 summarizes the atomic concentrations obtained from the XPS multiplex spectra acquired at a takeoff angle of 75° for the three hexapeptide films as well as their expected theoretical bulk values. Because a takeoff angle of 75° corresponds to a large XPS sampling depth, the atomic concentrations obtained from XPS should be very similar to the bulk values for thin films with monolayer coverage. As shown in Table 1, the experimental values agreed well with the theoretical bulk values. Figure 3 shows the typical photoelectron peaks and the associated curve-fittings for the elements detected in the hexapeptide films. The binding energies are summarized in Table 2. Table 3 lists the atomic ratios of the curve-fit derived components in the C1s and O1s windows. The C1s peak contained three components: the methyl and methylene carbon at 285.0 eV, the C–N/C–O peak at 286.4 eV, and the carbonyl carbon at 288.3 eV. The slight excess of the methyl and methylene carbon could be attributed to adventitious carbon adsorbed on the film surfaces. The O1s peak had two components: the carbonyl oxygen at 531.9 eV and C–O oxygen at 533.8 eV. In all the films, the lower than theoretical amount observed for the carbonyl (Table 3) is equivalent to a somewhat larger than theoretical value for the higher binding energy O1s component (at 533.8 eV). And this might be caused by the adsorbed water that could contribute to the higher binding energy component. The N1s binding energy was 400.1 eV, consistent with an amide functional group. All the above binding energies correlated well with the functional groups in the hexapeptides.<sup>40</sup> As seen in Figure 3, the signal-to-noise ratio for the S2p peak was poor due to its low atomic concentration. Nevertheless, its binding energy could be observed at around 162.5 eV, which was in agreement with a reported value for thiolate species on gold, suggesting chemisorbed sulfur.<sup>31,41</sup> No signal due to physisorbed sulfur (164 eV) was observed.

**Film Thickness and Stability.** The film thickness was calculated according to eq 1 and the values are summarized in Table 4. Because  $\lambda$  was obtained from a literature value,<sup>42,43</sup> it might not be very accurate. However, the thickness comparison between the films can yield useful information. The apparent thickness of the hexapeptide B and hexapeptide C SAMs was about 4 times that of the physisorbed hexapeptide A film, indicating greater film coverage in the SAMs due to the chemisorption via the disulfide moiety. In the physisorbed film, because there was no specific chemical interaction between the

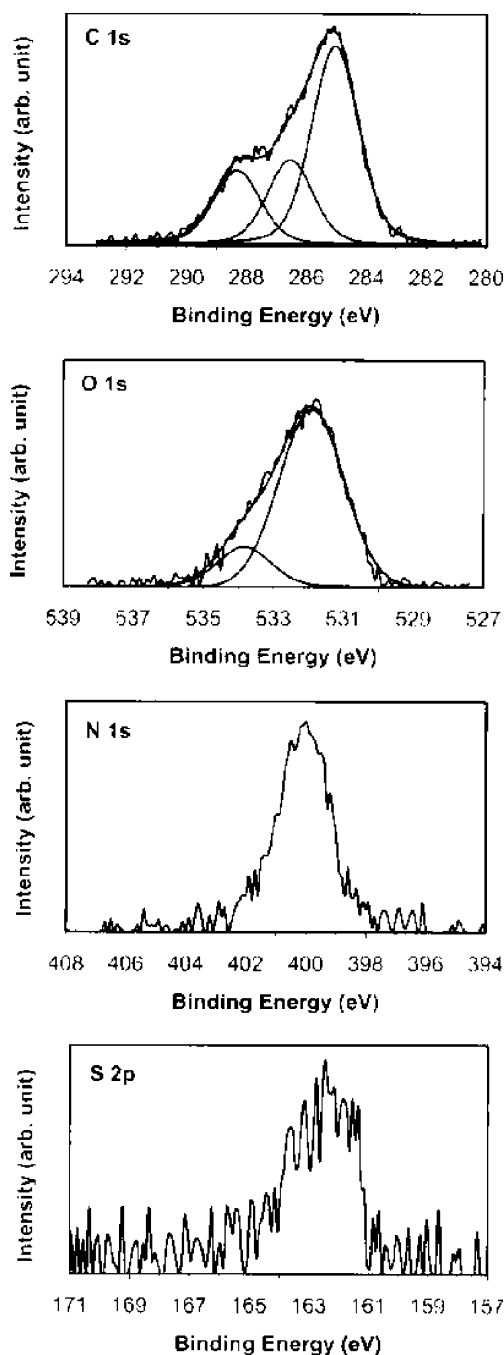


**Figure 3.** Representative XPS spectra of C1s, O1s, N1s, and S2p for hexapeptide films acquired at a takeoff angle of 75°.

gold substrate and hexapeptide A, most physisorbed hexapeptides were washed away during the solvent rinse, resulting in low film coverage, and thus apparently much thinner films. The FTIR–RAS spectra of the self-assembled hexapeptide B and physisorbed hexapeptide A films are shown in Figure 4. A comparison of the intensities of the amide I (around 1666  $\text{cm}^{-1}$ ) and amide II (around 1536  $\text{cm}^{-1}$ ) bands between the two films also indicated greater film coverage in the SAM hexapeptide film (Figure 4 top spectrum).

The stability of the self-assembled hexapeptide films in ethanol and dichloromethane was also investigated. The film thickness before and after a solvent soak is summarized in Table 4. Because the thickness difference between the self-assembled hexapeptide films without and with 1 week solvent soaks was very small (within the experimental error), the results suggested

**TABLE 2: XPS Binding Energies for Self-Assembled Hexapeptide B and Hexapeptide C Films and Physisorbed Hexapeptide A Film**

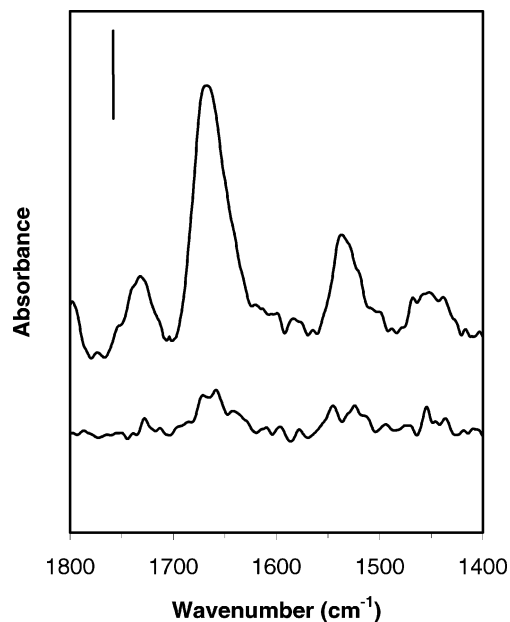
atom	functional group	binding energy (eV)		
		peptide B film	peptide C film	peptide A film
C 1s	methyl and methylene C	285.0	285.0	285.0
	C–N, C–O	286.4 ± 0.1	286.4 ± 0.1	286.3 ± 0.1
	C=O	288.3 ± 0.1	288.2 ± 0.1	288.4 ± 0.1
O 1s	C=O	531.9 ± 0.2	531.8 ± 0.1	532.0 ± 0.2
	C–O	533.8 ± 0.2	533.6 ± 0.2	533.9 ± 0.2
N 1s		400.1 ± 0.1	400.0 ± 0.1	400.2 ± 0.1
S 2p		162.5 ± 0.4	162.8 ± 0.3	
Au 4f <sub>7/2</sub>		83.9 ± 0.1	84.0 ± 0.1	83.8 ± 0.1

**TABLE 3: Ratios of Curve-Fit Components in the XPS C1s and O1s Windows Acquired at a Take-Off Angle of 75° for Self-Assembled Hexapeptide B and Hexapeptide C Films and Physisorbed Hexapeptide A Film**

film	methyl and methylene C	C		O	
		C–N, C–O	C=O	C=O	C–O
peptide B	3.29	1.02	1	6.77	1
theory	3.14	1	1	7	1
peptide C	3.55	1.32	1	3.38	1
theory	3.43	1.29	1	3.5	1
peptide A	3.11	1.12	1	3.29	1
theory	3	1.14	1	3.5	1

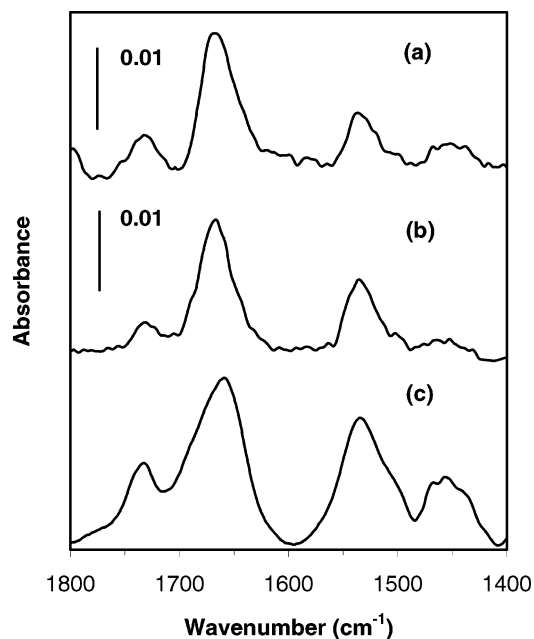
**TABLE 4: Film Thickness (nm) Obtained from XPS for Hexapeptide Films without and with One-week Solvent Soak**

film	without solvent soak (nm)	with 1-week solvent soak in EtOH (nm)	with 1-week solvent soak in CH <sub>2</sub> Cl <sub>2</sub> (nm)
peptide B	1.7 ± 0.2	1.6 ± 0.2	1.6 ± 0.3
peptide C	1.5 ± 0.2	1.3 ± 0.1	1.4 ± 0.2
peptide A	0.4 ± 0.1		

**Figure 4.** Grazing angle FTIR–RAS spectra of a self-assembled hexapeptide B film (top) and a physisorbed hexapeptide A film (bottom). The vertical scale bar is 0.01.

that the chemisorption between the hexapeptides and gold surface was robust in the presence of solvent.

**Hexapeptide Conformation and Orientation.** The conformation of the peptides in the SAMs was investigated by FTIR–RAS. Figure 5 shows the FTIR–RAS spectra of the self-

**Figure 5.** FTIR–RAS spectra of (a) a self-assembled hexapeptide B film and (b) a self-assembled hexapeptide C film. (c) Transmission FTIR spectrum of hexapeptide B in a KBr pellet.

assembled hexapeptide B and hexapeptide C films as well as the transmission spectrum of a hexapeptide B KBr pellet. The absorptions around 1666 and 1536 cm<sup>-1</sup> in the spectra of the self-assembled hexapeptide films were assigned to amide I and amide II bands, respectively. The wavenumber of the amide I band was slightly greater than that observed in an  $\alpha$ -helical conformation (1659 cm<sup>-1</sup>),<sup>44</sup> whereas the wavenumber of the amide II band was slightly lower than that observed in an  $\alpha$ -helical conformation (1540 cm<sup>-1</sup>).<sup>44</sup> The wavenumber difference may be attributed to the fact that hexapeptide B and hexapeptide C contain mixtures of  $3_{10}$ - and  $\alpha$ -helices. It is well-known that C $_{\alpha}$ -tetrasubstituted  $\alpha$ -amino acids such as Aib can promote the onset of  $3_{10}$ -helix formation.<sup>45</sup> Studies of hexapeptides known to form stable  $3_{10}$ -helices revealed that amide I and amide II bands occurred at 1666–1662 and 1533–1531 cm<sup>-1</sup>, respectively.<sup>29,34</sup> As a result, the observed amide I and amide II bands may be convolutions of the  $\alpha$ - and  $3_{10}$ -helical conformations. The bands around 1732 and 1450 cm<sup>-1</sup> were assigned to the ester C=O stretch and CH<sub>3</sub> asymmetrical in-plane deformation/CH<sub>2</sub> in-plane deformation, respectively.

ADXPS was used to study the depth profiles of both the self-assembled and physisorbed hexapeptide films. In ADXPS, the spectrum is more surface sensitive at smaller takeoff angles. Parts a and b of Figure 6 show the depth profiles of the self-assembled hexapeptide B and hexapeptide C films. Both the C/S and C/Au ratios decreased as the takeoff angle was increased, whereas C/O and C/N ratios were fairly constant and agreed well with the theoretical bulk ratios. Because the attenuation of the sulfur signal with varying takeoff angles followed the same trend as that of the gold signal and the attenuation of both signals was larger at smaller takeoff angles, the results indicated that the hexapeptides were bonded to the gold surface through the sulfur moieties and these were, in turn, buried beneath the hexapeptide backbone. The attenuation of the sulfur signal was due to the presence of hexapeptide backbones that were positioned above the disulfide moieties, so the results also suggested that the hexapeptide backbones were on average tilted up from the substrate surface and not lying flat on the gold surface. Compared to the self-assembled

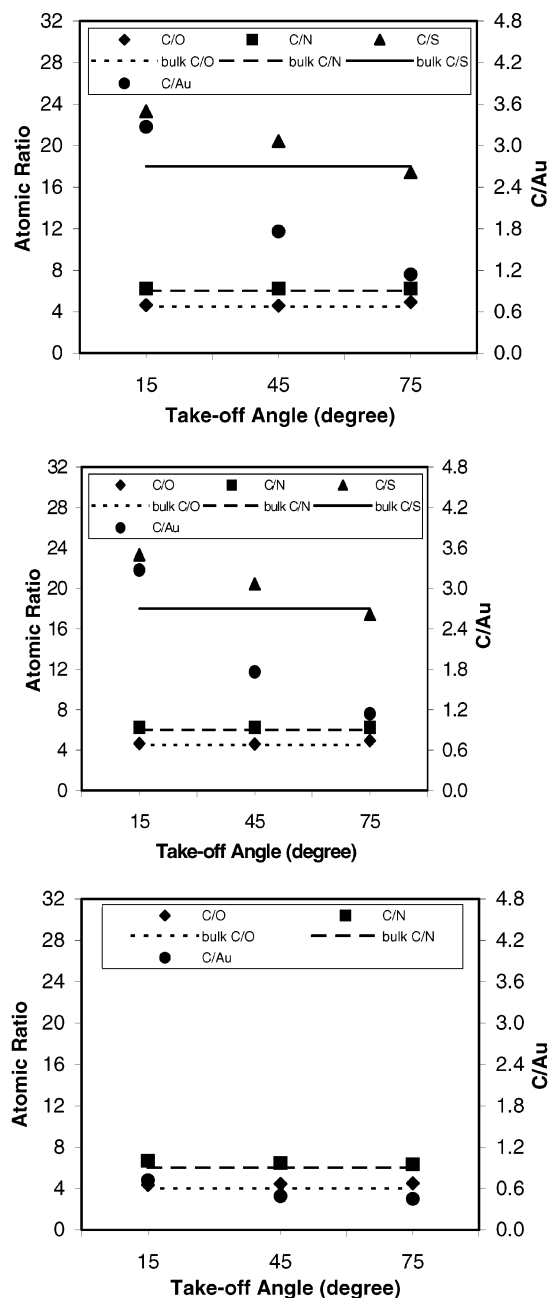


**Figure 6.** ADXPS depth profiles of (a) a self-assembled hexapeptide B film, (b) a self-assembled hexapeptide C film, and (c) a physisorbed hexapeptide A film.

hexapeptide films, the attenuation of the gold signal at smaller takeoff angles in the physisorbed film (Figure 6c) was much smaller. This was due to two reasons: First, the film coverage in the physisorbed film was smaller, so the substrate signal was less attenuated. Second, the hexapeptides in the physisorbed film were probably lying flat on the surface, resulting in a thinner film.

The orientation of the hexapeptide helix axis was also studied by FTIR–RAS. As shown in Figure 5, the amide I to amide II absorbance ratios were increased in the hexapeptide B and hexapeptide C SAM films compared to that in a hexapeptide KBr pellet. (Peptides in a KBr pellet were assumed to take random orientations.) The results suggested that the hexapeptides were on average oriented relative to the surface normal because the absorbance of the amide I band (with a transition moment parallel to the helix axis) was enhanced and the absorbance of the amide II band (with a transition moment perpendicular to

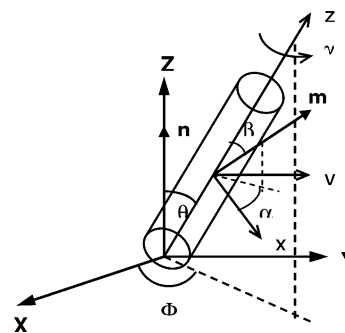


**Figure 7.** Coordinates of the laboratory ( $X, Y, Z$ ) and molecular ( $x, y, z$ ) systems for a tilted hexapeptide on gold surface.

the helix axis) was decreased, in accordance with the FTIR–RAS surface selection rule.<sup>46</sup>

**Orientation Distribution of hexapeptide Helix Axis on Gold.** The orientation of the adsorbate molecule within the SAM is determined by several factors such as the adsorbate–substrate binding strength, the geometry of the binding site, the intermolecular interactions between the adsorbed molecules, and the solvent–adsorbate interactions.<sup>1,47</sup> As a result of these factors, the orientation of the hexapeptide helix axis will be distributed about the substrate's surface normal. An orientation distribution function is necessary to generally interpret the FTIR–RAS spectrum and derive the average tilt angle from band intensities. Thus, we employ a Gaussian orientation distribution function to infer the hexapeptide helix axis orientation in the SAM on gold.<sup>14</sup> The helix axis orientation was obtained by optimizing the agreement between theoretical values for the amide I to amide II absorbance ratio,  $D$  (see eq 6), and the observed  $D$  value from the FTIR–RAS experiments.

Figure 7 shows the coordinate system that describes the interaction between the polarized, incident IR electric field and the molecular transition moment in the grazing angle FTIR–RAS experiment. Due to the surface selection rule,<sup>46</sup> the only active electric field component of the incident light ( $\mathbf{n}$ ) is parallel to the  $Z$ -axis of the laboratory system ( $X, Y, Z$ ); and the gold surface is in the  $X$ – $Y$  plane. The transition moment  $\mathbf{m}$  (amide I or amide II band) is located in a molecule (helix)-fixed frame ( $x, y, z$ ) by its respective polar and azimuthal angles ( $\alpha, \beta$ ). The  $x, y, z$  frame is oriented with the  $z$ -axis along the helix, and that axis is located in the laboratory system by  $\theta$ , and  $\Phi$ ;  $\gamma$  is the azimuthal angle about the helix axis. Using the relations among the Euler angles,<sup>48</sup> the projection of  $\mathbf{m}$  on  $\mathbf{n}$  is given by

$$\mathbf{m} \cdot \mathbf{n} = -\sin(\beta) \cos(\alpha) \sin(\theta) \cos(\gamma) + \sin(\beta) \sin(\alpha) \sin(\theta) \sin(\gamma) + \cos(\beta) \cos(\theta) \quad (2)$$

The FTIR–RAS absorption intensity,  $A$ , is proportional to  $|\mathbf{m} \cdot \mathbf{n}|^2$ . Assuming uniform azimuthal distribution about the helix axis— $\gamma$  is uniformly distributed over the interval  $[0, 2\pi]$ —we find

$$A \propto \langle |\mathbf{m} \cdot \mathbf{n}|^2 \rangle_\gamma = \frac{1}{2} - \frac{1}{2} \cos^2(\theta) - \frac{1}{2} \cos^2(\beta) + \frac{3}{2} \cos^2(\beta) \cos^2(\theta) \quad (3)$$

(The  $\alpha$ -dependence is simultaneously averaged by this assumption for  $\gamma$ .) As the angles between the transition moment and the helix axis were determined to be  $39^\circ$  for  $\beta_1$  (amide I band) and  $75^\circ$  for  $\beta_2$  (amide II band),<sup>49</sup>  $A$  can be written as  $A(\theta)$ , where  $\theta$  describes the tilt angle between the helix axis and the surface normal.

The observed FTIR–RAS absorption intensity ( $A_{\text{obs}}$ ) depends on the orientation distribution of the helices in the film. Thus,  $A_{\text{obs}}$  is the weighted superposition of contributions,  $A(\theta) W(\theta) d\theta$ , where  $W(\theta)$  is the normalized helix axis orientation distribution function. Hence, we have

$$A_{\text{obs}} = \int_0^{\pi} A(\theta) W(\theta) d\theta \propto \int_0^{\pi} \langle |\mathbf{m} \cdot \mathbf{n}|^2 \rangle_{\gamma} W(\theta) d\theta \quad (4)$$

Similarly, the average of any function  $X$  of the tilt angle of the helix axis relative to the surface normal is

$$\langle X \rangle = \int_0^{\pi} X(\theta) W(\theta) d\theta \quad (5)$$

The amide I to amide II absorbance ratio is

$$D = K \frac{A_{\text{obs}}^{\text{I}}}{A_{\text{obs}}^{\text{II}}} = K \frac{\int_0^{\pi} \langle |\mathbf{m} \cdot \mathbf{n}|^2 \rangle_{\gamma}^{\text{I}} W(\theta) d\theta}{\int_0^{\pi} \langle |\mathbf{m} \cdot \mathbf{n}|^2 \rangle_{\gamma}^{\text{II}} W(\theta) d\theta} \quad (6)$$

where  $K$  is the scaling factor that relates the intrinsic “oscillator strength” of the amide I and amide II vibrational modes.  $K$  was determined to be 1.35 from the transmission FTIR spectrum of a hexapeptide KBr pellet.

The Gaussian orientation distribution function that is used to model the helix axis orientation distribution is

$$W(\theta) = N^{-1} \exp\left[-\frac{1}{2\sigma^2}(\theta - \theta_0)^2\right] \sin(\theta) \quad (7)$$

where  $N$  is the normalization constant:

$$N = \int_0^{\pi} \exp\left[-\frac{1}{2\sigma^2}(\theta - \theta_0)^2\right] \sin(\theta) d\theta \quad (8)$$

The orientation distribution function is centered at  $\theta_0$  ( $=0^\circ$  for helices oriented normal to the substrate) with the angular spread of the distribution specified by  $\sigma$ . The Gaussian function is weighted by the factor  $\sin(\theta)$  to account for azimuthal degeneracy of the helix axis tilt about the surface normal. But one might argue that azimuthal disorder, i.e., a hemispherical distribution of helix axes according to eqs 7 and 8, is inappropriate for a SAM composed of domains having uniform helix tilt throughout. This can be easily rectified by removing the degeneracy factor, i.e., setting  $\sin(\theta) = 1$  in eqs 7 and 8. We denote the former and latter distributions as hemispherical Gaussian (HG) and uniform-domain Gaussian (UDG), respectively.

Figure 8 shows the results for calculated  $D$  values using eqs 2–8 (dotted lines) for a range of values of the tilt angle  $\theta_0$  ( $=0$ – $50^\circ$ ) as a function of the spread of the distribution  $\sigma$  ( $=0$ – $90^\circ$ ), using both the HG (Figure 8a) and UDG distributions (Figure 8b); the gray planes correspond to  $D = 2.95$ , and  $D = 2.63$ , the observed value for amide I to amide II absorbance ratio for SAMs prepared from hexapeptide B and C, respectively (Table 5). For both distributions it is apparent from Figure 8 that there is not a unique solution—a specific tilt corresponding to the observed  $D$  value for either SAM. In fact, there is a locus of points where the  $D$  planes intersect the computed  $D$  values (indicated by solid lines on the respective planes) that span a wide range of qualitatively different solutions. In the ideal case of perpendicular orientation of the helix axes relative to the substrate ( $\theta_0 = 0^\circ$ ), a fit to the observations is obtained only for a broad distribution ( $\sigma \sim 35^\circ$  and  $\sim 70^\circ$  for the HG and

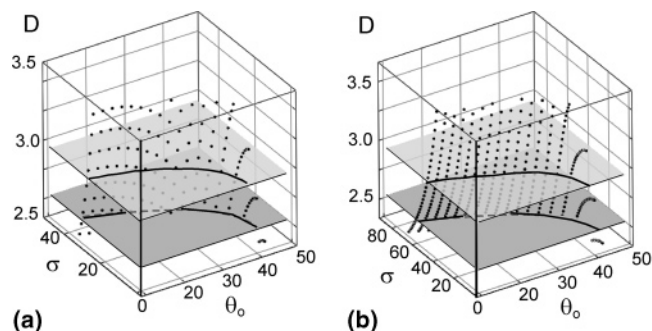


**Figure 8.** Amide I to amide II absorbance ratio  $D$ . Dotted lines are calculated  $D$  values as a function of tilt angle  $\theta_0$  and distribution spread  $\sigma$ ; the two planes correspond to the observed  $D$  values (2.95 and 2.63) for hexapeptides B and C, respectively. (a)  $D$  values computed with the hemispherical Gaussian (HG) distribution. (b)  $D$  values computed with the uniform-domain Gaussian (UDG) distribution.

**TABLE 5: Amide I to Amide II Absorbance Ratio  $D$  Obtained from FTIR–RAS for Self-Assembled Hexapeptide B and Hexapeptide C Films**

film	amide I/amide II <sup>a</sup> $D$
peptide B	$2.95 \pm 0.24$
Peptide C	$2.63 \pm 0.13$

<sup>a</sup> The values were the averages of four different samples.

**TABLE 6: Hexapeptide Length Obtained from Molecular Modeling and Calculated Film Thickness for Self-Assembled Hexapeptide B and Hexapeptide C Films<sup>a</sup>**

film	model length $L_m$ (nm)	film thickness from XPS $L$ (nm)
peptide B	2.21	$1.7 \pm 0.2$
peptide C	2.24	$1.5 \pm 0.2$

<sup>a</sup> The calculated film thickness is compared to that obtained from XPS.

UDG distributions, respectively). At the other extreme, one can fit  $D$  with a very tight distribution ( $\sigma \sim 0^\circ$ ), i.e., find a “unique” value for the helix axis tilt relative to the surface normal, for a tilt  $\theta_0 \sim 35$ – $45^\circ$  for each distribution. (When contrasting parts a and b of Figures 8, note the scale differences for  $\sigma$ .) In summary, though there is a shift in the locus of the fits to the observed  $D$  values on changing the HG distribution to the UDG distribution, there remains significant ambiguity in those fits—no single tilt value  $\theta_0$  is a unique solution, and a range of options for  $\theta_0$  can be chosen by varying the breadth of the tilt disorder ( $\sigma$ ).

In the same way, the average SAM film thickness,  $\langle L \rangle$ , can be calculated with both orientation distributions,

$$\langle L \rangle = \int_0^{\pi} L_m \cos(\theta) W(\theta) d\theta \quad (9)$$

where  $L_m$  is the ideal hexapeptide length (determined from molecular modeling). The ideal  $L_m$  values and the experimentally derived film thickness for SAM films formed from hexapeptides B and C are given in Table 6. The experimental film thicknesses were determined from XPS and correspond to the planes shown in Figure 9. Again the ambiguity one observed for  $D$  applies to  $\langle L \rangle$  for both the HG distribution (eq 7) and the UDG distribution (eq 7 without the  $\sin(\theta)$  factor). In the absence of any compelling additional evidence these results suggest that for monodisperse hexapeptides, either the helices are broadly distributed about the substrate normal in the SAMs or there are a range of tilt values  $\theta_0$  and corresponding distribution breadths  $\sigma$  that can explain the experimentally observed  $D$  values and  $L$  values.

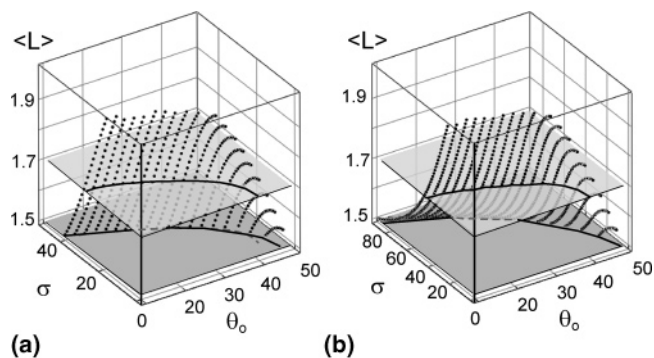


**Figure 9.** SAM film thickness. Dotted lines are calculated  $\langle L \rangle$  values as a function of tilt angle  $\theta_0$  and distribution spread  $\sigma$ . The two planes correspond to the observed  $L$  values (1.7 and 1.5 nm) for hexapeptides B and C, respectively. (a)  $\langle L \rangle$  values computed with the hemispherical Gaussian (HG) distribution. (b)  $\langle L \rangle$  values computed with the uniform-domain Gaussian (UDG) distribution.

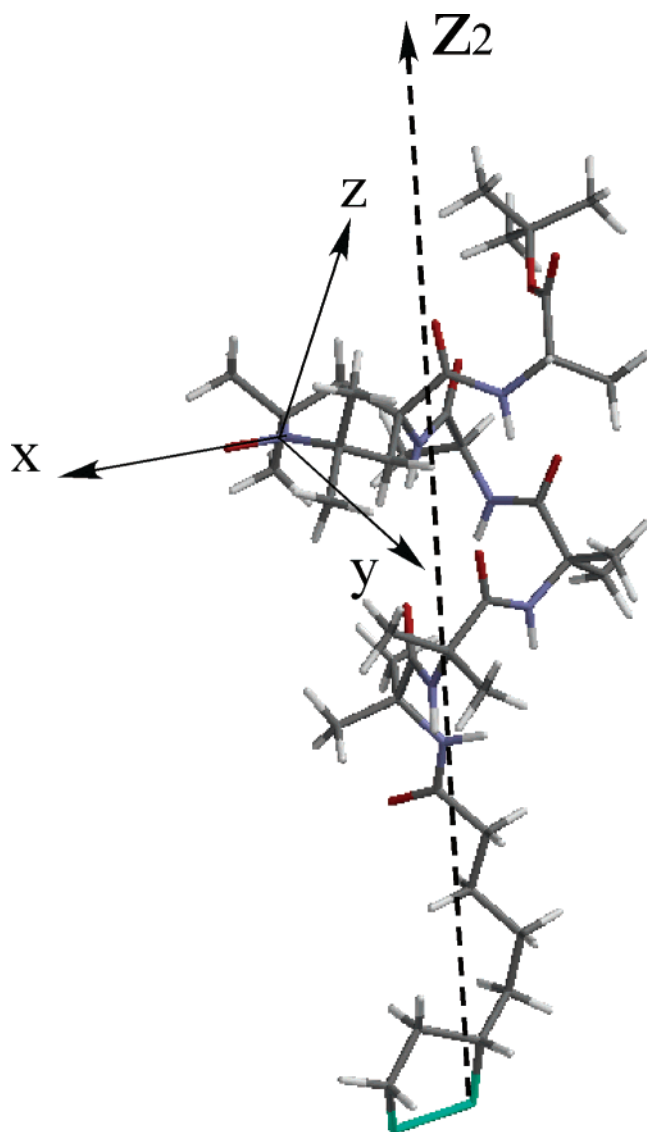


**Figure 10.** 2,2,6,6-Tetramethylpiperidine-1-oxyl-4-amino-4-carboxylic acid (TOAC)-labeled hexapeptide C showing the fragment-fixed  $x$ ,  $y$ ,  $z$  frame that diagonalizes the  $g$ - and  $A$ -tensors of the free radical. The  $x$ -axis is along the  $N-O$  bond and  $z$  is normal to the  $>N-O$  plane;  $z_2$  is the helix axis.

**SAMs Composed of TOAC-Labeled Hexapeptides.** The TOAC residue, a nitroxide radical, constitutes a bulky peptide side chain. SAMs composed of hexapeptide C are not as thick

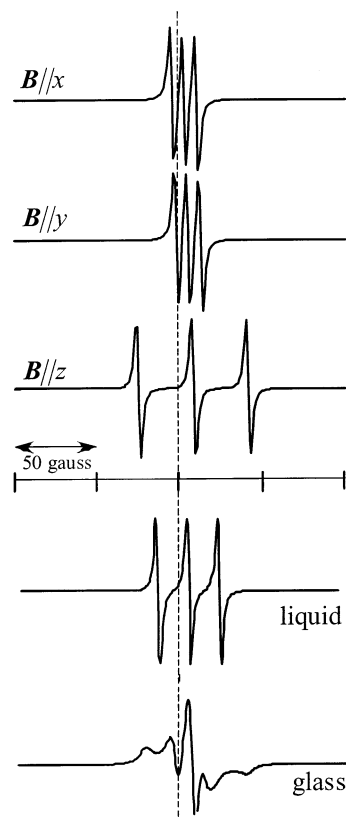


**Figure 11.** Simulated ESR spectra for the TOAC free radical. The top three spectra are computed with the spectrometer magnetic field  $\mathbf{B}$  along the axes of the  $x$ ,  $y$ ,  $z$  principal axis system of the TOAC radical. The solution spectrum corresponds to a motionally averaged spectrum, and the glass is a static powder spectrum.

as SAMs from hexapeptide B, even though  $L_m$  for hexapeptide C (2.24 nm) is marginally larger than that of hexapeptide B (2.21 nm). Also the observed value for amide I to amide II absorbance ratio for hexapeptide C is smaller (Tables 4 and 5). The results suggested that the packing in the TOAC-labeled hexapeptide SAM was more disordered than that in the SAM composed of hexapeptide B.

**Electron Spin Resonance.** ESR was used to study the local order in the hexapeptide C SAM. The  $g$ - and  $A$ -tensor components of the TOAC nitroxide radical are well-known. The  $g$ -tensor and hyperfine coupling tensor,  $A$ , coincide with a local ( $x$ ,  $y$ ,  $z$ ) principal axis system (PAS) having the  $N-O$  bond along the  $x$ -axis and the  $z$ -axis along the nitrogen and oxygen  $2p$  orbitals that contain the unpaired electron; the  $y$ -axis completes the local Cartesian PAS (Figure 10). In  $x$ ,  $y$ ,  $z$  both  $g$  and  $A$  are diagonal with principal values  $g_{xx}$ ,  $g_{yy}$ ,  $g_{zz}$  (2.0096, 2.0064, 2.0027) and  $A_{xx}$ ,  $A_{yy}$ ,  $A_{zz}$  (7.455 G, 7.455 G, 33.3 G); studies by Hanson et al.<sup>50</sup> using this TOAC hexapeptide show that the  $x$ ,  $y$ ,  $z$  PAS frame is rotated about its  $x$ -axis by  $68^\circ$  to give  $g$  and  $A$  in an  $x_2$ ,  $y_2$ ,  $z_2$  frame fixed on the helix with  $z_2$  along the helix axis; the  $x$  and  $x_2$  axes are coincident and oriented normal to the helix  $z_2$ -axis. To simulate ESR spectra, it is necessary to transform  $g$  and  $A$  to the laboratory  $X$ ,  $Y$ ,  $Z$  frame (with the ESR spectrometer magnetic field  $\mathbf{B}$  along  $Z$ ). Simulated ESR spectra and their relationship to the helix axis distribution in the SAM is carried out via an intermediate transformation to a SAM-fixed  $X_1$ ,  $Y_1$ ,  $Z_1$  frame having the  $Z_1$ -axis normal to the substrate.<sup>51</sup>

We assume that the TOAC label is in the rigid limit with reorientational correlation time  $\tau \gg 10^{-8}$  s (at 9.5 GHz,  $\tau \gg \{[A_{zz} - A_{xx}]^{-1} \approx \{h|g_{xx} - g_{zz}|\beta_e \mathbf{B}\}^{-1} \approx 10^{-8}$  s, where  $\beta_e$  is the

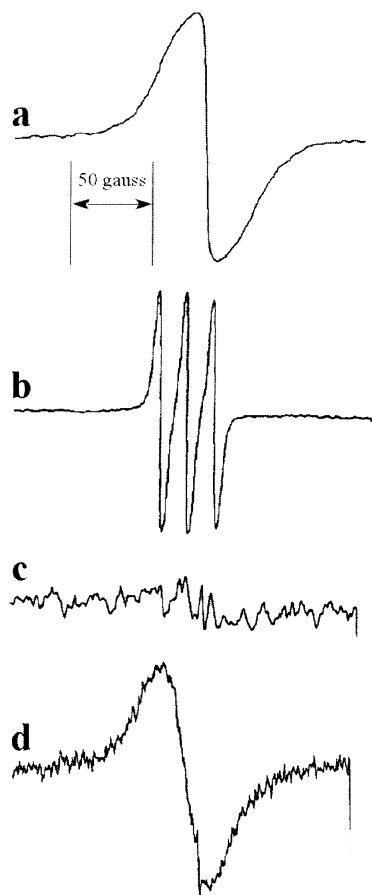


**Figure 12.** Experimental ESR spectra for the TOAC-labeled hexapeptide at room temperature: (a) solid sample; (b) solution (20 mM in benzene); (c) physisorbed hexapeptide on gold substrate (no detectable signal); (d) SAM of hexapeptide C on gold (substrate normal along field **B**).

electron Bohr magneton). The ideal static spectra for a perfectly oriented nitroxide radical with **B** along each of the respective axes of the local PAS are shown at the top of Figure 11. The simulated spectra for a solid isotropic glass and a motionally averaged liquid ( $\tau \ll 10^{-8}$  s) are also shown.

Experimental ESR spectra obtained with the TOAC-labeled hexapeptide are shown in Figure 12. The neat solid sample of hexapeptide C exhibits an ESR spectrum (Figure 12a) that was rather broad without the clearly defined hyperfine splittings (unresolved **g**- and **A**-tensor components unlike the ideal glass spectrum in Figure 11). The collapse of the hyperfine structure is not surprising and is due to spin–spin exchange caused by a high local concentration of TOAC radicals. In contrast, the solution spectrum of the TOAC-labeled polypeptide was well resolved (Figure 12b) and showed the expected hyperfine structure, a resolved triplet. There is basically no detectable signal from samples where the TOAC-labeled hexapeptide is physisorbed on gold (Figure 12c). Whereas for the SAM (Figure 12d) a spin-exchanged broadened spectrum is observed.

In an attempt to reduce the local concentration of TOAC radicals and resolve fine structure in the ESR spectra of the self-assembled hexapeptide, a SAM in which the ratio of TOAC-labeled hexapeptide C was diluted by unlabeled hexapeptide B (dilution ratio 1:9) was prepared. The ESR spectrum of the diluted SAM (Figure 13) shows a somewhat narrower spectrum with indications of fine structure. However, the ESR spectra of the diluted SAM did not show any angular dependence as was the case in the spin-labeled fatty acid SAMs.<sup>52,53</sup> We observed a lack of ESR evidence for a biased distribution of the principal

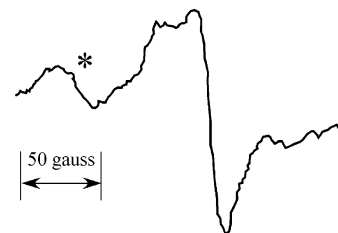


**Figure 13.** Experimental ESR spectra for the TOAC-labeled hexapeptide SAM of hexapeptide C diluted 10-fold by hexapeptide B (on gold with substrate normal along field **B**). \* indicated a background resonance in the ESR cavity.

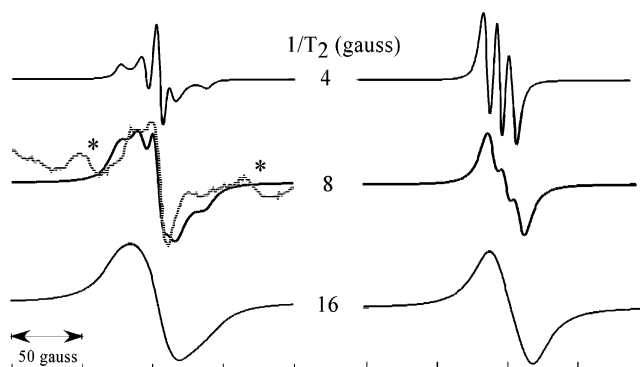


**Figure 14.** Simulated ESR spectra for the TOAC-labeled hexapeptides for different line widths ( $1/T_2$ ). (Left) HG distribution ( $\sigma = 90^\circ$ ). This is tantamount to an isotropic distribution of radicals. (Right) UDG distribution ( $\theta_0 = 35^\circ$ ,  $\sigma = 10^\circ$ ). The experimental ESR spectrum (Figure 13) is superposed on the  $1/T_2 = 8$  G line width spectrum for the HG distribution. \* indicates cavity background signals.

axes of the **g**- and **A**-tensors; i.e., the apparent anisotropy of the TOAC orientation was low in the diluted SAM. In the absence of spin-exchange broadening, simulations of ESR spectra using the HG and UDG distributions could in principle differentiate between tight helix axis distributions (small  $\sigma$ ) about a well-defined tilt angle  $\theta_0$ , and disordered helix orientations (or isotropically distributed nitroxide radicals) within the SAM. This discriminatory capability of ESR is shown in the simulations in Figure 14 (top) for the case where the line width ( $1/T_2 = 4$  G) is small (simulations using the HG distribution are on the left and those using the UDG distribution are shown on the right). However, as the line width is increased to mimic spin-exchange broadening, one rapidly begins to lose the ability to discriminate between the HG and UDG distributions. The qualitative agreement between the experimental spectrum of the dilute SAM and the  $1/T_2 = 8$  G simulation is best for a hemispherical distribution of nitroxide radicals (Figure 14). Insofar as this coarse agreement is meaningful, either it could result from an absence of helix axis orientational preferences in the dilute SAM or the apparent disorder could be due to an unraveling of the helix and associated disorder of the nitroxide side chain. Minimally, the ESR experiment is one more piece of evidence that a significant amount of the hexapeptide C was self-assembled on the gold substrate.

## Conclusions

Monodisperse Aib containing hexapeptides that had lipoic acid coupled to the N-terminus were able to form stable self-assembled monolayers on gold substrates. The film compositions agreed well with the expected bulk values. XPS results revealed that the surface coverage of the self-assembled films was significantly larger than that of the physisorbed films. The chemisorption between the terminal lipoic acid of the hexapep-



tide and the gold surface was stable in solvent, and it played an important role in the formation of the hexapeptide monolayers. The hexapeptides in the monolayers exhibited a mixed  $3_{10}/\alpha$ -helical conformation. ADXPS and FTIR–RAS results suggested that the hexapeptides were partially oriented. Modeling the helix axis orientation distribution to compute the amide I to amide II absorbance ratio  $D$  and the SAM thickness  $\langle L \rangle$  suggests that a wide range of parameters ( $\theta_0$  and  $\sigma$ ) satisfy the experimentally observed  $D$  and  $L$  values. Such ambiguity is avoided in grafted polypeptides where larger observed  $D$  values (3.5–7) restrict the range of parameters in the distributions. ESR results for SAMs composed of the TOAC-labeled hexapeptide exhibited too much spin-exchange broadening to derive useful structural information.

**Acknowledgment.** We thank Professor M. D. E. Forbes for advice and E. J. Harbron for help with the ESR experiments. This work was supported in part by the National Science Foundation (DMR-9412701) and by a NASA University Research, Engineering and Technology Institute on Bio Inspired Materials (BIMat) under award No. NCC-1-02037.

## References and Notes

- Ulman, A. *An Introduction to Ultrathin Organic Films: from Langmuir–Blodgett to Self-Assembly*; Academic Press: New York, 1991.
- Nuzzo, R. G.; Allara, D. L. *J. Am. Chem. Soc.* **1983**, *105*, 4481.
- Ulman, A. *Chem. Rev.* **1996**, *96*, 1533.
- Poirier, G. E. *Chem. Rev.* **1997**, *97*, 1117.
- Dishner, M. H.; Hemminger, J. C.; Feher, F. J. *Langmuir* **1996**, *12*, 6176.
- Tao, Y. T.; Pandiaraju, S.; Lin, W. L.; Chen, L. J. *Langmuir* **1998**, *14*, 145.
- Lukkari, J.; Meretoja, M.; Kartio, I.; Laajalehto, K.; Rajamäki, M.; Lindström, M.; Kankare, J. *Langmuir* **1999**, *15*, 3529.
- Schlenoff, J. B.; Li, M.; Ly, H. *J. Am. Chem. Soc.* **1995**, *117*, 12528.
- Schessler, H. M.; Karpovich, D. S.; Blanchard, G. J. *J. Am. Chem. Soc.* **1996**, *118*, 9645.
- Nuzzo, R. G.; Dubois, L. H.; Allara, D. L. *J. Am. Chem. Soc.* **1990**, *112*, 558.
- Chidsey, C. E. D.; Liu, G. Y.; Rowntree, P.; Scoles, G. *J. Chem. Phys.* **1989**, *91*, 4421.
- Widrig, C. A.; Alves, C. A.; Porter, M. D. *J. Am. Chem. Soc.* **1991**, *113*, 2805.
- Enriquez, E. P.; Gray, K. H.; Guarisco, V. F.; Linton, R. W.; Mar, K. D.; Samulski, E. T. *J. Vac. Sci. Technol., A* **1992**, *10*, 2775.
- Enriquez, E. P.; Samulski, E. T. *Mater. Res. Soc. Symp. Proc.* **1992**, *255*, 423.
- Merrifield, B. *Science* **1986**, *232*, 341.
- Creel, H. S.; Fournier, M. J.; Mason, T. L.; Tirrell, D. A. *Macromolecules* **1991**, *24*, 1213.
- Miura, Y.; Kimura, S.; Kobayashi, S.; Iwamoto, M.; Imanishi, Y.; Umemura, J. *Chem. Phys. Lett.* **1999**, *315*, 1.
- Morita, T.; Kimura, S.; Kobayashi, S.; Imanishi, Y. *J. Am. Chem. Soc.* **2000**, *122*, 2850.
- Kimura, S.; Miura, Y.; Morita, T.; Kobayashi, S.; Imanishi, Y. *J. Polym. Sci. A: Polym. Chem.* **2000**, *38*, 4826.
- Whitesell, J. K.; Chang, H. K. *Science* **1993**, *261*, 73.
- Chang, Y.; Frank, C. W. *Langmuir* **1996**, *12*, 5824.
- Heise, A.; Menzel, H.; Yim, H.; Foster, M. D.; Wieringa, R. H.; Achouten, A. J.; Erb, V.; Stamm, M. *Langmuir* **1997**, *13*, 723.
- Worley, C. G.; Linton, R. W.; Samulski, E. T. *Langmuir* **1995**, *11*, 3805.
- Fujita, K.; Bunjes, N.; Nakajima, K.; Hara, M.; Sasabe, H.; Knoll, W. *Langmuir* **1998**, *14*, 6167.
- Miura, Y.; Kimura, S.; Imanishi, Y.; Umemura, J. *Langmuir* **1998**, *14*, 6935.
- Miura, Y.; Kimura, S.; Imanishi, Y.; Umemura, J. *Langmuir* **1998**, *14*, 2761.
- Miura, Y.; Kimura, S.; Imanishi, Y.; Umemura, J. *Langmuir* **1999**, *15*, 1155.
- Buggess, A. W.; Leach, S. J. *Biopolymers* **1973**, *12*, 2599.
- Karle, I. L.; Balaram, P. *Biochemistry* **1990**, *29*, 6747.
- Veciana, J.; Iwamura, H. *MRS Bull.* **2000**, *25*, 41.
- Bain, C. D.; Biebuyck, H. A.; Whitesides, G. M. *Langmuir* **1989**, *5*, 723.
- Fabianowski, W.; Colye, L. C.; Weber, B. A.; Granata, R. D.; Castner, D. G.; Sadownik, A.; Regen, S. L. *Langmuir* **1989**, *5*, 35.
- Toniolo, C.; Bonora, G. M.; Barone, V.; Bavoso, A.; Benedetti, E.; Blasio, B. D.; Grimaldi, P.; Lelj, F.; Pavone, V.; Pedone, C. *Macromolecules* **1985**, *18*, 895.
- Kennedy, D. F.; Crisma, M.; Toniolo, C.; Chapman, D. *Biochemistry* **1991**, *30*, 6541.
- Hanson, P.; Millhauser, F.; Formaggio, F.; Crisma, M.; Toniolo, C. *J. Am. Chem. Soc.* **1996**, *118*, 7618.
- Flippen-Anderson, J. L.; George, C.; Valle, G.; Valente, E.; Bianco, A.; Formaggio, F.; Crisma, M.; Toniolo, C. *Int. J. Peptide Protein Res.* **1996**, *47*, 231.
- Handbook of X-ray Photoelectron Spectroscopy*; Chastain, J., Ed.; Perkin-Elmer Corp.: Eden Prairie, MN, 1992.
- Shirley, D. A. *Phys. Rev. B* **1972**, *5*, 4709.
- Fadey, C. S. *Prog. Surf. Sci.* **1984**, *16*, 3.
- NIST X-ray Photoelectron Spectroscopy Database Version 2.0 NIST Standard Reference Database 20*; U.S. Department of Commerce: Gaithersburg, MD, 1997.
- Nuzzo, R. G.; Zegarski, B. R.; Dubois, L. H. *J. Am. Chem. Soc.* **1987**, *109*, 773.
- Laibinis, P. E.; Bain, C. D.; Whitesides, G. M. *J. Phys. Chem.* **1991**, *95*, 7017.
- Bain, C. D.; Whitesides, G. M. *J. Phys. Chem.* **1989**, *93*, 1670.
- Krimm, S.; Bandeker, J. *Adv. Protein Chem.* **1986**, *38*, 181.
- Toniolo, C.; Benedetti, E. *Trends Biochem. Sci.* **1991**, *16*, 350.
- Greenler, R. G. *J. Chem. Phys.* **1966**, *44*, 310.
- Swalen, J. D. *Annu. Rev. Mater. Sci.* **1991**, *21*, 373.
- Michl, J.; Thulstrup, E. W. *Spectroscopy with Polarized Light: Solute Alignment by Photoselection, in Liquid Crystals, Polymers, and Membranes*; VCH Publishers: Deerfield Beach, FL, 1986.
- Tsuboi, M. *J. Polym. Sci.* **1965**, *59*, 139.
- Hanson, P. et al. *Mol. Phys.* **1998**, *95*, 957.
- Pan, S. P.; Birrell, G. B.; Griffith, O. H. *J. Magn. Reson.* **1974**, *15*, 444.
- Risse, T.; Hill, T.; Schmidt, J.; Abend, G.; Hamann, H.; Freund, H.-J. *J. Phys. Chem. B* **1998**, *102*, 2668.
- Wieringa, R. H.; Siesling, E. A.; Werkman, P. J.; Angerman, H.; J.; Vorenkamp, E. J.; Schouten, A. J. *Langmuir* **2001**, *17*, 6485.